JOC The Journal of Organic Chemistry

Article

pubs.acs.org/joc

Factors Governing the Diels–Alder Reactivity of (2,7)Pyrenophanes

Yago García-Rodeja and Israel Fernández*

Departamento de Química Orgánica I and Centro de Innovación en Química Avanzada (ORFEO–CINQA), Facultad de Ciencias Químicas, Universidad Complutense, 28040 Madrid, Spain

Supporting Information

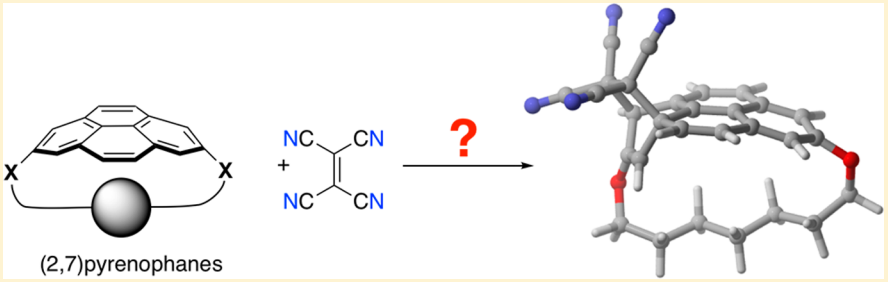

ABSTRACT: The physical factors governing the Diels–Alder reactivity of (2,7)pyrenophanes have been computationally explored using state-of-the-art Density Functional Theory calculations. It is found that the [4 + 2]-cycloaddition reactions between these cyclophanes and tetracyanoethylene, which occur concertedly through highly asynchronous transition states, proceed with lower activation barriers and are more exothermic than the analogous process involving the parent planar pyrene. The influence of the bent equilibrium geometry of the pyrenophane as a function of the length of the bridge as well as the nature of the tether on the transformation are analyzed in detail. By means of the Activation Strain Model of reactivity and the Energy Decomposition Analysis methods, a detailed quantitative understanding of the reactivity of this particular family of cyclophanes is presented.

INTRODUCTION

Cyclophanes are characterized by having an aliphatic chain that bridges two nonadjacent positions of an aromatic ring. Since the isolation of the first cyclophane, the archetypical [2.2]paracyclophane, by Brown and Farthing in 1949,[1] the chemistry of this family of compounds has experienced tremendous development.[2] Indeed, cyclophanes are nowadays ubiquitous species in different fields of organic and organometallic chemistry such as, for instance, asymmetric catalysis,[3] supramolecular chemistry,[4] or materials science.[5]

Among the vast number of cyclophanes prepared so far, pyrene-based cyclophanes, also known as pyrenophanes, have attracted much attention recently.[6] This is due to not only the extraordinary photophysical and photochemical properties of this particular polycyclic aromatic hydrocarbon[7] but also its importance as a key structural unit for the preparation of large curved π-organic materials.[6,8] For these reasons, a good number of pyrenophanes having (1,3), (1,6), (1,7), (1,8), (2,4), (2,7), and (4,9) bridging motifs have been prepared and fully characterized.[6] However, although considerable efforts toward the synthesis and structural analyses of these compound have been made,[6,9] their chemistry remains comparatively underdeveloped. Thus, only a few reactions including Diels–Alder cycloadditions,[9b,10] and some unusual processes involving *t*-BuLi and alkali metals,[11] have been reported so far. This is somewhat surprising if we take into account that the synthesis of pyrenophane derivatives may provide access to novel species with significant potential applications in the above commented fields.

Herein, we have focused on the Diels–Alder reactivity of (2,7)pyrenophanes. Bodwell and co-workers reported that [*n*](2,7)pyrenophanes **1** and 1,*n*-dioxa[n](2,7)pyrenophanes **2** undergo [4 + 2]-cycloaddition reactions with reactive dienophiles such as tetracyanoethylene (TCNE) or 4-phenyl-1,2,4-triazoline-3,5-dione (PTAD) at room temperature (Scheme 1).[9b,10] Interestingly, whereas pyrenophanes with n = 7 (**1-m5** and **2-m5**) easily react with TCNE, the next-higher counterparts (n = 8, for instance, **2-m6** in Scheme 1a) are both unreactive even when heating at 80 °C. A similar reactivity trend was observed in the reactions with PTAD (see Scheme 1b). Although it was suggested that the strain relief in the transformation is likely responsible for this behavior, the physical factors behind the observed different Diels–Alder reactivities are so far not fully understood.

Fortunately, the introduction of the so-called Activation Strain Model (ASM)[12] of reactivity in combination with the Energy Decomposition Analysis (EDA)[13] method has allowed us to quantitatively understand the factors governing different fundamental processes in organic chemistry[14,15] as well as metal-mediated transformations.[16] This approach has been particularly useful to our current understanding of the Diels–Alder reactions involving fullerenes[17] as well as planar and bowl-

Received: June 12, 2017
Published: July 11, 2017

DOI: 10.1021/acs.joc.7b01449
J. Org. Chem. 2017, 82, 8157–8164

Scheme 1. Diels–Alder Reactions Involving (2,7)Pyrenophanes 1 and 2 (TCNE = Tetracyanoethylene, PTAD = 4-Phenyl-1,2,4-triazoline-3,5-dione)

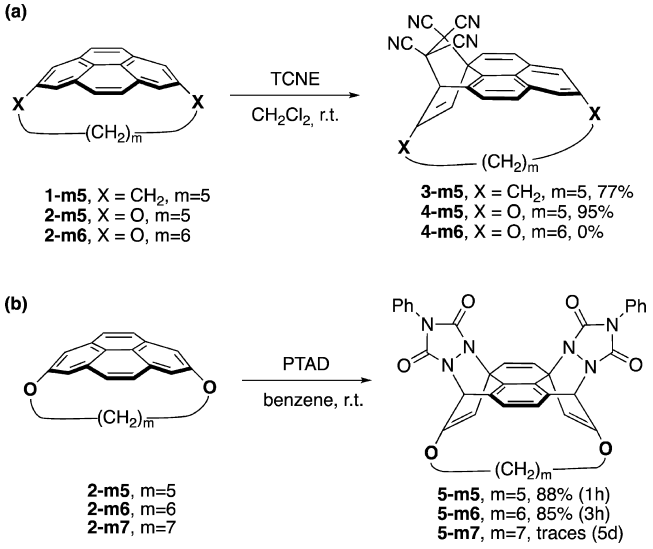

shaped polycyclic aromatic hydrocarbons, species which are strongly related to the (2,7)pyrenophanes considered herein.[18] Therefore, in this study we report the application of the ASM method to gain a deeper, quantitative insight into the Diels–Alder reactivity of this particular family of cyclophanes. Issues such as the influence of the length of the aliphatic bridge connecting the positions 2 and 7 of the pyrene nucleus as well as the nature of the tether on the transformation will be also analyzed in detail.

THEORETICAL METHODS

Computational Details. All the calculations reported in this paper were obtained with the GAUSSIAN 09 suite of programs.[19] All reactants, transition structures, and cycloadducts were optimized using the B3LYP functional[20] in conjunction with the D3 dispersion correction suggested by Grimme et al.[21] using the double-ζ quality def2-SVP basis sets[22] for all atoms. All stationary points were characterized by frequency calculations.[23] Reactants and cycloadducts have positive definite Hessian matrices, whereas transition structures (TSs) show only one negative eigenvalue in their diagonalized force constant matrices, and their associated eigenvectors were confirmed to correspond to the motion along the reaction coordinate under consideration using the Intrinsic Reaction Coordinate (IRC) method.[24] Single-point calculations at the M06-2X[25] level using the triple-ζ quality plus polarization def2-TZVPP basis set[22] for all atoms were performed on the optimized geometries to refine the computed energies. Solvent effects (solvent = benzene) were taken into account during the single-point calculations using the Polarizable Continuum Model (PCM).[26] This level is denoted PCM(benzene)-M06-2X/def2-TZVPP//B3LYP-D3/def2-SVP.

Activation Strain Analyses of Reaction Profiles. The *activation strain model*,[12] also known as *distortion/interaction model*,[27] is a fragment approach to understanding chemical reactions, in which the height of reaction barriers is described and understood in terms of the original reactants. Within this approach, the potential energy surface $\Delta E(\zeta)$ is decomposed, along the reaction coordinate ζ, into two contributions, namely the strain $\Delta E_{strain}(\zeta)$ associated with deforming the individual reactants plus the actual interaction $\Delta E_{int}(\zeta)$ between the deformed reactants (eq 1):

$$\Delta E(\zeta) = \Delta E_{strain}(\zeta) + \Delta E_{int}(\zeta) \quad (1)$$

The strain $\Delta E_{strain}(\zeta)$ is typically determined by the rigidity of the reactants and to the extent at which groups must reorganize in a particular reaction mechanism, whereas the interaction $\Delta E_{int}(\zeta)$ between the reactants depends on their electronic structure and on how they are mutually oriented as they approach each other. It is the interplay between $\Delta E_{strain}(\zeta)$ and $\Delta E_{int}(\zeta)$ that determines if and at which point along ζ a barrier arises (i.e., at the point where $d\Delta E_{strain}(\zeta)/$

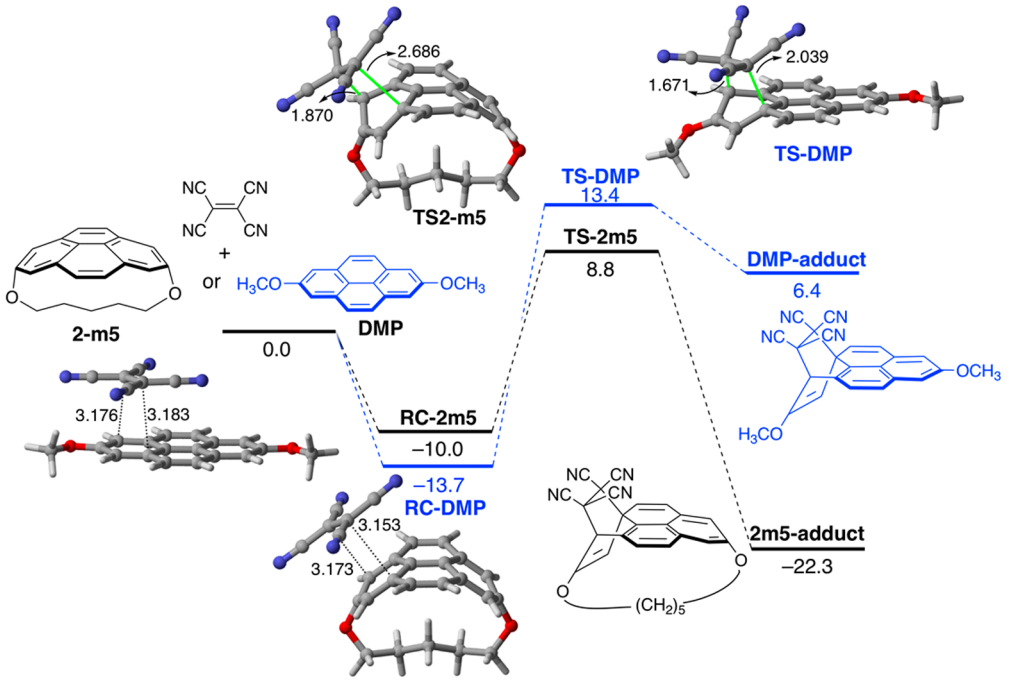

Figure 1. Computed reaction profiles for the Diels–Alder reactions between (2,7)pyrenophane **2-m5** and 2,7-dimethoxypyrene (DMP) with TCNE. Relative energies and bond distances are given in kcal/mol and angstroms, respectively. All data have been computed at the PCM(benzene)-M06-2X/def2-TZVPP//B3LYP-D3/def2-SVP level.

DOI: 10.1021/acs.joc.7b01449
J. Org. Chem. 2017, 82, 8157–8164

$d\zeta = -d\Delta E_{int}(\zeta)/d\zeta$). The activation energy of a reaction $\Delta E^{\ddagger} = \Delta E(\zeta^{TS})$ consists therefore of the activation strain $\Delta E_{strain}{}^{\ddagger} = \Delta E_{strain}(\zeta^{TS})$ plus the TS interaction $\Delta E_{int}{}^{\ddagger} = \Delta E_{int}(\zeta^{TS})$:

$$\Delta E^{\ddagger} = \Delta E_{strain}{}^{\ddagger} + \Delta E_{int}{}^{\ddagger} \quad (2)$$

Herein, the reaction coordinate is defined as the projection of the IRC on the shortest forming C···C distance between the carbon atom of the pyrenophane and the carbon atom of TCNE. This reaction coordinate ζ undergoes a well-defined change in the course of the reaction from ∞ to the equilibrium C···C distance in the corresponding transition structures.

RESULTS AND DISCUSSION

We first compared the [4 + 2]-cycloaddition reactions of the 1,7-dioxa[7](2,7)pyrenophane **2-m5** and the parent 2,7-dimethoxypyrene (DMP) with TCNE to understand the influence of the curvature imposed in the cyclophane on the transformation. As readily seen in Figure 1, our calculations indicate that in both cases the reaction proceeds via the exothermic formation of an initial reactant complex which is transformed into the corresponding cycloadduct in a concerted manner through the transition states **TS-2m5** and **TS-DMP**, respectively. These saddle points are associated with the simultaneous, albeit highly asynchronous, formation of both C−C bonds, a feature also shared by related planar and bowl-shaped polycyclic aromatic hydrocarbons.[18] From the data in Figure 1, it becomes clear that the cycloaddition reaction involving the pyrenophane is both kinetically ($\Delta\Delta E^{\ddagger}$ = 8.3 kcal/mol) and thermodynamically ($\Delta\Delta E_R$ = 15.9 kcal/mol) favored over the analogous process involving the parent planar DMP. This can be initially ascribed to the bent equilibrium geometry of **2-m5** which (i) is greatly relieved in the corresponding cycloadduct and (ii) better fits into the transition state structure as compared to the planar DMP. As a result, the transition state **TS-2m5** is reached much earlier than the analogous **TS-DMP** (see Figure 1).

Further quantitative insight into the reasons behind the much lower activation barrier associated with the process involving the cyclophanes can be gained by means of the Activation Strain Model (ASM) of reactivity. Figure 2 shows the computed activation strain diagrams (ASD) for the above cycloaddition reactions from the corresponding initial reactant complexes up to the respective transition states. Not surprisingly, it is found that the strain energy computed for the process involving **2-m5** is clearly lower (i.e., less destabilizing) than that for the reaction involving the parent DMP along the entire reaction coordinate. For instance, at the transition state structures, a value of ΔE_{strain} = 49.4 kcal/mol was computed for the reaction involving the pyrenophane whereas a much higher (i.e., more destabilizing) value of ΔE_{strain} = 103.9 kcal/mol was computed for the parent process involving DMP (Figure 2). This is of course a direct consequence of the bent equilibrium geometry of **2-m5** which requires less deformation to adopt the transition state geometry as compared to the planar DMP. Therefore, although the interaction energy is even slightly stronger for the DMP reaction (see Figure 2), it can be concluded that the strain energy is the main factor controlling the lower activation barrier computed for the [4 + 2]-cycloaddition reaction involving (2,7)pyrenophane **2-m5**. A similar finding was also observed not only in the related [4 + 2]-cycloadditions between bowl-shaped polycyclic aromatic hydrocarbons and cyclopentadiene[18a] but also in the [3 + 2]-cycloaddition reactions involving group 14 heteroallenes and triple bonds.[28]

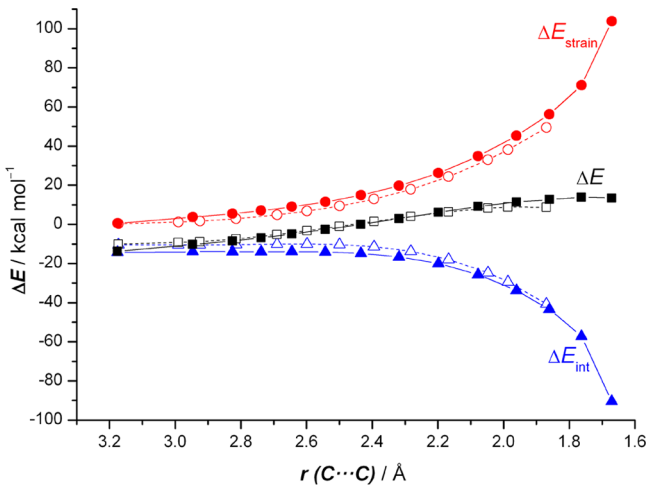

Figure 2. Comparative activation-strain diagrams of the [4 + 2]-cycloaddition reactions between TCNE and 2,7-dimethoxypyrene (solid lines) and (2,7)pyrenophane **2-m5** (dashed lines) along the reaction coordinate projected onto the forming C···C bond distance. All data have been computed at the PCM(benzene)-M06-2X/def2-TZVPP//B3LYP-D3/def2-SVP level.

Influence of the Length of the Bridge. In order to investigate the effect of the length of the tether on the Diels−Alder reactivity of (2,7)pyrenophanes, we considered the [4 + 2]-cycloaddition reactions between TCNE and 1,*n*-dioxa[*n*](2,7)-pyrenophanes **2** (*n* = 5 to 10; see Table 1).

Table 1 gathers the activation barriers, reaction energies, and activation strain data of the considered Diels−Alder cycloaddition reactions at the PCM(benzene)M06-2X/def2-TZVPP//B3LYP-D3/def2-SVP level. In all cases, it is found that the transformation begins with an initial reactant complex (located at ca. −10 kcal/mol below the separate reactants) which is transformed into the respective cycloadducts through the concerted and asynchronous transition states **TS2** (see also Figure 3). Regardless of the length of the bridge, the process involving pyrenophanes **2** is systematically easier from a kinetic point of view ($\Delta E^{\ddagger}$ in the range of 16.9 to 24.3 kcal/mol) and more exothermic ($\Delta E^{\ddagger}$ in the range of −3.7 to −32.9 kcal/mol) than the analogous cycloaddition involving the parent DMP. Despite that, there is a smooth convergence to the DMP barrier and reaction energies if the length of the tether is increased. Thus, the activation barrier energy becomes higher and the cycloaddition becomes less exothermic as the length of the aliphatic bridge becomes longer. This effect can be once again ascribed to the equilibrium geometry of the pyrenophane reactant, which steadily becomes increasingly more bent as the length of the tether becomes shorter. Indeed, good linear relationships between the activation barriers as well as the reaction energies and the curvature of the pyrenophane (measured by the geometrical parameter *h*, see Figure 4 for a definition) were found (correlation coefficients of 0.95 and 0.96, respectively, Figure 4), which confirms the crucial role of the bent geometry of the pyrenophane on the process. Please note that the computed barrier and reaction energies computed for **2-m6**, the next-higher homologue of **2-m5**, are not that unfavorable as compared to the data computed for **2-m5**. Therefore, the experimentally observed lack of reactivity of this species should be attributed to an experimental issue rather than to the intrinsic reactivity of **2-m6** (indeed, this species is able to undergo the analogous Diels−Alder reaction with PTAD; see Scheme 1).[10]

DOI: 10.1021/acs.joc.7b01449
J. Org. Chem. 2017, 82, 8157−8164

Table 1. Computed Energies (in kcal/mol, PCM(Benzene)-M06-2X/def2-TZVPP//B3LYP-D3/def2-SVP Level) for the Diels–Alder Cycloaddition Reactions between TCNE and (2,7)Pyrenophanes 2

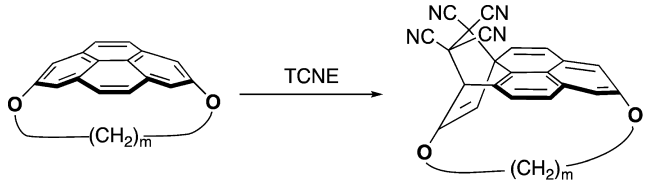

2-mx (m = 3 to 8) **adduct-2-mx (m = 3 to 8)**

compd	m	ΔE_{RC} [a]	$\Delta E^{\ddagger}$ [b]	ΔE_R [c]	$\Delta E_{strain,TCNE}^{\ddagger}$ [d]	$\Delta E_{strain,2\text{-}mx}^{\ddagger}$ [e]	$\Delta E_{strain}^{\ddagger}$ [f]	$\Delta E_{int}^{\ddagger}$ [g]	h [h]
2-m3	3	−9.5	16.9	−32.9	20.7	23.2	43.9	−36.5	2.125
2-m4	4	−9.8	17.6	−30.0	21.6	23.0	44.6	−36.8	1.922
2-m5	5	−10.0	18.8	−22.3	23.5	25.9	49.4	−40.6	1.659
2-m6	6	−10.1	19.2	−14.2	30.0	30.3	60.3	−51.2	1.332
2-m7	7	−10.5	21.4	−7.1	37.9	42.1	80.0	−69.1	1.086
2-m8	8	−10.7	24.3	−3.7	38.2	43.9	82.1	−68.6	0.800
DMP	–	−13.7	27.1	6.4	51.3	52.6	103.9	−90.5	0.000

[a]Reactant complex (**RC**) energy: $\Delta E_{RC} = E_{RC} - E$(pyrenophane/DMP) $- E$(TCNE). [b]Activation energy: $\Delta E^{\ddagger} = E(\mathbf{TS}) - E(\mathbf{RC})$. [c]Reaction energy: $\Delta E_R = E$(cycloadduct) $- E$(pyrenophane/DMP) $- E$(TCNE). [d]$\Delta E_{strain,TCNE}^{\ddagger} = E_{TCNE}(\mathbf{TS}) - E_{TCNE}$. [e]$\Delta E_{strain,2\text{-}mx}^{\ddagger} = E_{2\text{-}mx}(\mathbf{TS}) - E_{2\text{-}mx}$. [f]$\Delta E_{strain}^{\ddagger} = \Delta E_{strain,TCNE}^{\ddagger} + \Delta E_{strain,2\text{-}mx}^{\ddagger}$. [g]$\Delta E_{int}^{\ddagger} = E(\mathbf{TS}) - E_{TCNE}(\mathbf{TS}) - E_{2\text{-}mx}(\mathbf{TS})$. [h]$h$ values (in Å, for a definition see Figure 4).

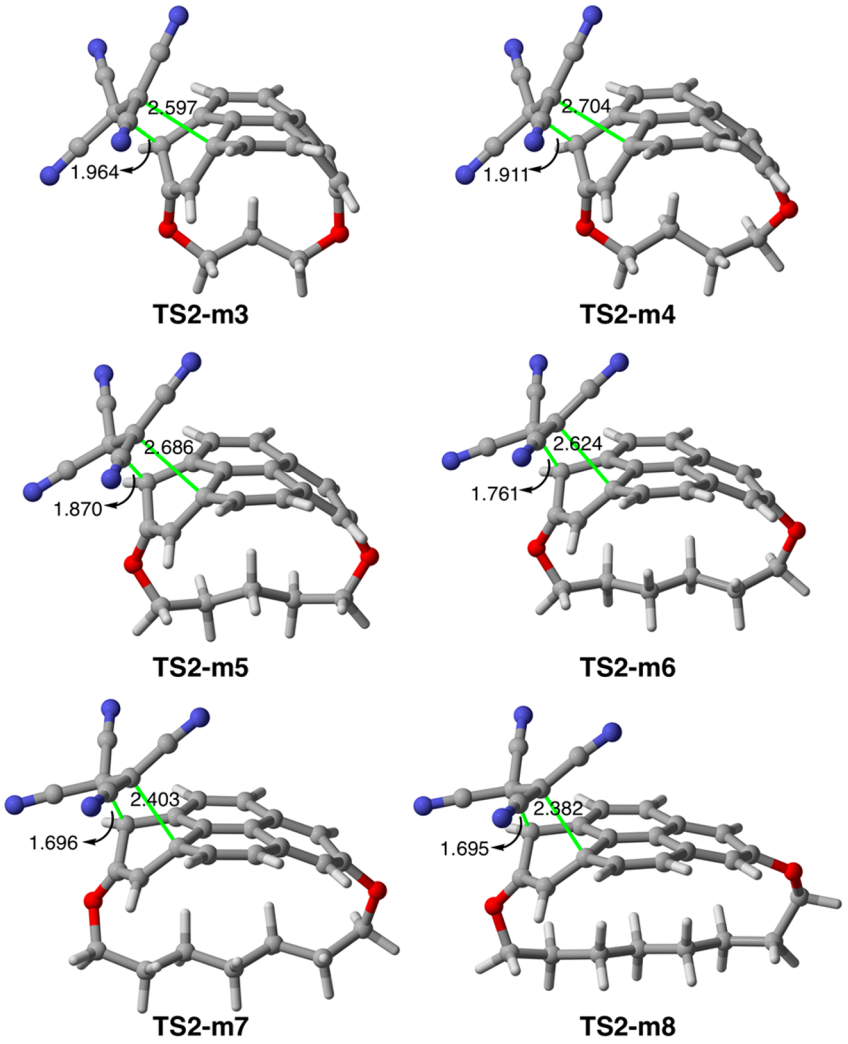

Figure 3. Fully optimized geometries (B3LYP-D3/def2-SVP level) of the transition states involved in the Diels–Alder cycloaddition reactions between TCNE and (2,7)pyrenophanes **2** (m = 3 to 8). Bond distances are given in angstroms.

Not surprisingly, the ASM of reactivity indicates that the activation strain energy, $\Delta E_{strain}^{\ddagger}$, follows the same trend as the activation barrier; i.e., processes with higher barriers are associated with higher deformation energies (see Table 1).

DOI: 10.1021/acs.joc.7b01449
J. Org. Chem. 2017, 82, 8157–8164

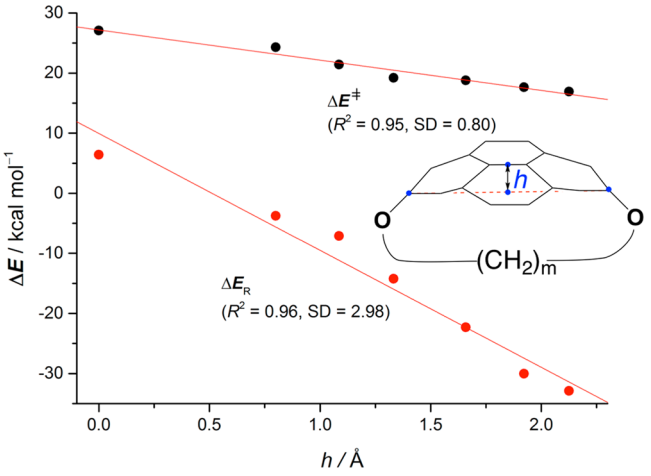

Figure 4. Plot of the activation barriers ($\Delta E^{\ddagger}$) and reaction energies (ΔE_R) versus the curvature parameter h. Inset: geometrical definition of parameter h (defined as the distance between the center of the bond connecting the central C3a[1] and C5a[1] atoms and the center of the line connecting C2 and C7 atoms).

This finding provides further support to the above conclusion about the crucial role of the initial curvature of the pyrenophane on the cycloaddition. Therefore, cyclophanes with high h values (i.e., having shorter tethers) already possess a bent equilibrium geometry which better fits into the corresponding transition state structure. As a consequence, these species require less deformation and, as a result, lower activation barriers. As expected, a good linear correlation was found when plotting the computed $\Delta E_{strain}^{\ddagger}$ vs $\Delta E^{\ddagger}$ (correlation coefficient of 0.93, Figure 5), which confirms that the [4 + 2]-cycloaddition reactions

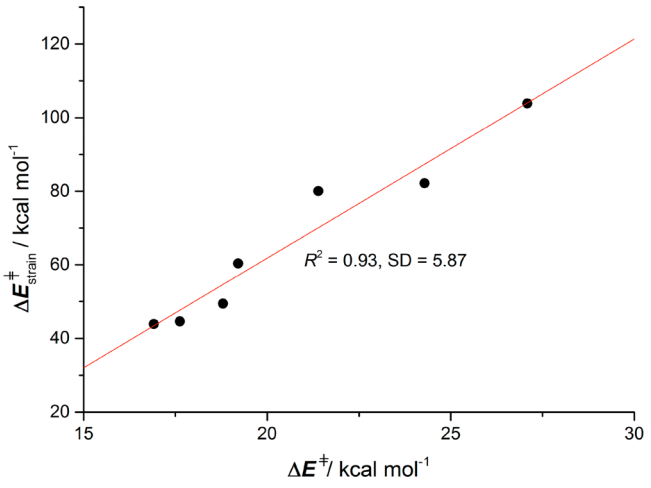

Figure 5. Plot of the barrier energies ($\Delta E^{\ddagger}$) versus activation strain energies ($\Delta E_{strain}^{\ddagger}$) for the Diels–Alder cycloaddition reactions between TCNE and pyrenophanes **2** and 2,7-dimethoxypyrene. Energy values were computed at the PCM(benzene)-M06-2X/def2-TZVPP//B3LYP-D3/def2-SVP level.

involving (2,7)pyrenophanes are mainly controlled by the energy required by the cyclophane to adopt the geometry of the corresponding transition state. In this sense, it is not surprising either that the transition states associated with lower barriers (with higher h values and shorter bridges) are reached earlier than those associated with higher barriers (having lower h values and longer bridges; see Figure 3).

Influence of the Nature of the Tether. We finally were curious to analyze the effect of the presence of an aryl group in the bridge of (2,7)pyrenophanes on the [4 + 2]-cycloaddition reaction with TCNE. Although compound **6-H** (Table 2) was also prepared by Bodwell and co-workers,[29] nothing is known about its reactivity.

Table 2. Computed Energies (in kcal/mol, PCM(Benzene)-M06-2X/def2-TZVPP//B3LYP-D3/def2-SVP level) for the Diels–Alder Cycloaddition Reactions between TCNE and (2,7)Pyrenophanes 6

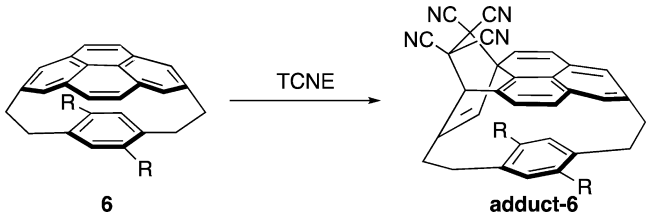

6 **adduct-6**

compd	ΔE_{RC}[a]	$\Delta E^{\ddagger}$[b]	ΔE_R[c]	h[d]
6-H	−11.4	18.9	−15.3	1.358
6-NH$_2$	−12.3	17.6	−14.8	1.348
6-OMe	−11.9	18.3	−14.8	1.357
6-CN	−10.4	20.2	−12.0	1.327
6-F	−10.8	20.3	−13.4	1.328

[a]Reactant complex (**RC**) energy: $\Delta E_{RC} = E_{RC} - E$(pyrenophane) − E(TCNE). [b]Activation energy: $\Delta E^{\ddagger}$ = E(**TS**) − E(**RC**). [c]Reaction energy: $\Delta E_R = E$(cycloadduct) − E(pyrenophane) − E(TCNE). [d]h values (in Å, for a definition see Figure 4).

The computed curvature value h for **6-H** is 1.358 Å (Table 2). This value is higher than that computed for the analogous all-carbon tethered (2,7)pyrenophane, i.e. having eight CH_2 moieties connecting the positions 2 and 7 of the pyrene (h = 1.207 Å), and as a consequence, the computed activation barrier is lower ($\Delta E^{\ddagger}$ = 18.9 vs 19.5 kcal/mol). Moreover, the h value of **6-H** is rather similar to that computed for the 1,6-dioxa[6](2,7)-pyrenophanes **2-m6** (h = 1.332 Å, see Table 1). However, the computed activation barrier for the cycloaddition involving **6-H** does not resemble that for **2-m6** but for the next-lower homologue **2-m5** ($\Delta E^{\ddagger}$ = 18.9 vs 18.8 kcal/mol)[30] despite the latter species possessing a more bent equilibrium geometry (h = 1.659 Å). This suggests that, in addition to the curvature, there should be another factor which enhances the Diels–Alder reactivity of this particular pyrenophane. Indeed, application of the NCIPLOT method[31] reveals the occurrence of a strong noncovalent π–π attractive interaction between the aryl fragment and the pyrene moiety (Figure 6). We hypothesize that this intramolecular interaction makes the pyrene fragment a better diene and, consequently, enhances the interaction between the pyrenophane and the dienophile TCNE.

To support this hypothesis, we modified the electronic nature of the aryl fragment by introducing substituents at the adjacent positions to the carbon atoms involved in the aromatic bridge. Clearly, the presence of good π-donor substituents such as NH_2 groups (compound **6-NH$_2$**) further enhances the Diels–Alder reactivity of the system in view of the lower computed activation barrier of 17.6 kcal/mol (Table 2). Note that this species presents a curvature h value of 1.348 Å, which is even lower (i.e., less bent) than that for **6-H**, which highlights the importance of the π–π intramolecular interaction (Figure 6). A similar reactivity enhancement is found for the dimethoxy-substituted

DOI: 10.1021/acs.joc.7b01449
J. Org. Chem. 2017, 82, 8157–8164

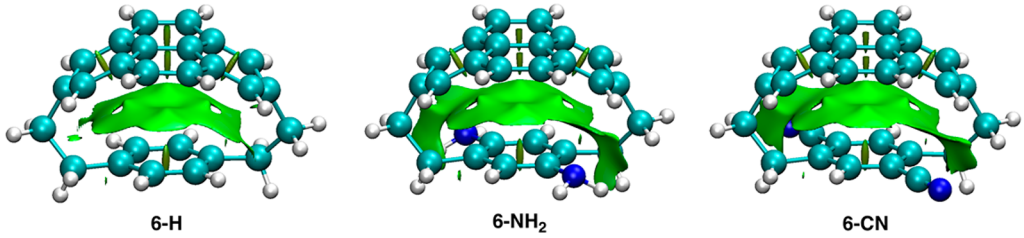

Figure 6. Contour plots of the reduced density gradient isosurfaces (density cutoff of 0.03 au) representing the noncovalent interactions in (2,7)-pyrenophanes **6-H**, **6-NH$_2$**, and **6-CN**.

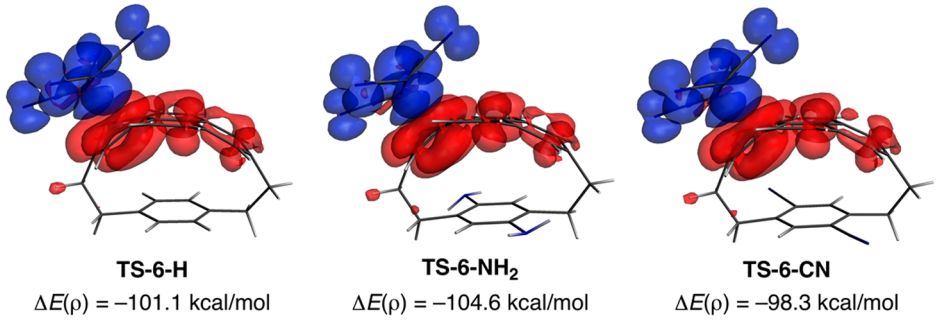

Figure 7. Plot of the deformation densities ($\Delta\rho$) of the pairwise orbital interactions between TCNE and pyrenophanes **6** and associated stabilization energies ($\Delta E(\rho)$, in kcal/mol). The color code of the charge flow is red → blue.

cyclophane **6-OMe** ($\Delta E^{\ddagger}$ = 18.3 kcal/mol). In contrast, the introduction of electron-withdrawing substituents such as CN groups (**6-CN**) leads to the opposite effect and a higher reaction barrier is computed for this species ($\Delta E^{\ddagger}$ = 20.2 kcal/mol, Table 2). A similar effect is found for **6-F**, possessing four fluorine atoms in the aryl fragment (see Table 2). Therefore, it can be concluded that the reactivity of pyrenophanes having an aryl fragment in their bridges is not exclusively governed by the extent of the curvature of their equilibrium geometries, as it occurs in their aliphatic counterparts. Intramolecular $\pi-\pi$ interactions must be also taken into account as they tune the electronic properties of the pyrene moiety.

Although the computed HOMO(pyrenophane)−LUMO(TCNE) gap qualitatively agrees with the computed reactivity trend: 0.64 eV (**6-F**) > 0.34 eV (**6-H**) > 0.08 eV (**6-NH$_2$**), we finally applied the NOCV (Natural Orbital for the Chemical Valence)[32] extension of the EDA method[13] to quantitatively assess the strength of the π(diene)$-\pi^*$(dienophile) orbital interaction in the cycloaddition.[33] From the data in Figure 7, which depicts the corresponding deformation densities ($\Delta\rho$) of the pairwise orbital interactions at the corresponding transition states, it becomes clear that this $\pi \rightarrow \pi^*$ interaction follows the same trend as that followed by the corresponding activation barriers: −104.6 kcal/mol (**6-NH$_2$**) > −101.1 kcal/mol (**6-H**) > −98.4 kcal/mol (**6-CN**). Therefore, it is quantitatively confirmed that the $\pi-\pi$ intramolecular interaction in these species does modify the electronic nature of the pyrene moiety and, consequently, the reactivity of the system. Thus, whereas electron-rich aryl groups in the tether make the pyrene−TCNE interaction stronger and, as a result, lead to lower activation barriers, the presence of electron-withdrawing groups provokes the opposite effect.

CONCLUSIONS

From the computational study reported herein, the following conclusions can be drawn: (i) similar to the process involving the parent 2,7-dimethoxypyrene, the Diels−Alder reactions between tetracyanoethylene and (2,7)pyrenophanes proceed concertedly through highly asynchronous transition states. (ii) Despite that, the processes involving pyrenophanes occur systematically with lower activation barriers and are more exothermic than the analogous cycloaddition reaction involving the parent DMP. (iii) This is mainly due to the fact that these cyclophanes already possess a bent geometry which better fits into the corresponding transition state geometry therefore requiring significant less deformation. (iv) Interestingly, there is a smooth convergence to the DMP barrier and reaction energies if the length of the tether of the cyclophane is increased. Thus, the barrier energy becomes higher and the cycloaddition becomes less exothermic as the length of the aliphatic bridge becomes longer. This is a direct consequence of the curvature of the pyrenophane, which becomes lower also when the length of the aliphatic bridge becomes longer. (v) Finally, in those species having an aromatic fragment in the tether, the Diels−Alder reactivity is not exclusively controlled by the curvature of the system. In these cases, there exists a remarkable intramolecular $\pi-\pi$ interaction between the aryl fragment and the pyrene moiety which does modify the electronic nature of the pyrene moiety and, consequently, the interaction between the pyrenophane and the dienophile TCNE and, ultimately, the activation barrier of the process.

ASSOCIATED CONTENT

Supporting Information

The Supporting Information is available free of charge on the ACS Publications website at DOI: 10.1021/acs.joc.7b01449.

Figure S1, Cartesian coordinates (in Å), and total energies (in a.u.) of all the stationary points discussed in the text (PDF)

AUTHOR INFORMATION

Corresponding Author

*E-mail: israel@quim.ucm.es.

DOI: 10.1021/acs.joc.7b01449
J. Org. Chem. 2017, 82, 8157−8164

ORCID

Israel Fernández: 0000-0002-0186-9774

Notes

The authors declare no competing financial interest.

■ ACKNOWLEDGMENTS

Financial support was provided by the Spanish Ministerio de Economía y Competitividad (MINECO) and FEDER (Projects CTQ2016-78205-P and CTQ2014-51912-REDC). Y.G.-R. acknowledges the MINECO for an FPI grant.

■ REFERENCES

(1) Brown, C. J.; Farthing, A. C. *Nature* **1949**, *164*, 915.
(2) (a) Diederich, F. *Cyclophanes*; Royal Society of Chemistry: Cambridge, U.K., 1991. (b) *Modern Cyclophane Chemistry*, Gleiter, R., Hopf, H., Eds.; Wiley-VCH: Weinheim, Germany, 2004.
(3) Selected representative examples: (a) Wack, H.; France, S.; Hafez, A. M.; Drury, W. D., III; Weatherwax, A.; Lectka, T. *J. Org. Chem.* **2004**, *69*, 4531. (b) Matsuoka, Y.; Ishida, Y.; Sasaki, D.; Saigo, K. *Chem. - Eur. J.* **2008**, *14*, 9215. (c) For a review focused on [2.2]paracyclophane derivatives, see: Paradies, J. *Synthesis* **2011**, *2011*, 3749.
(4) Recent examples: (a) Dale, E. J.; Vermeulen, N. A.; Juríček, M.; Barnes, J. C.; Young, R. M.; Wasielewski, M. R.; Stoddart, J. F. *Acc. Chem. Res.* **2016**, *49*, 262. (b) Fagnani, D. E.; Meese, M. J., Jr.; Abboud, K. A.; Castellano, R. K. *Angew. Chem., Int. Ed.* **2016**, *55*, 10726.
(5) See, for instance: (a) Bazan, G. C. *J. Org. Chem.* **2007**, *72*, 8615. (b) Morisaki, Y.; Murakami, T.; Chujo, Y. *Macromolecules* **2008**, *41*, 5960. (c) Jagtap, S. P.; Collard, D. M. *J. Am. Chem. Soc.* **2010**, *132*, 12208. (d) Morisaki, Y.; Chujo, Y. *Polym. Chem.* **2011**, *2*, 1249. (e) Jagtap, S. P.; Mukhopadhyay, S.; Coropceanu, V.; Brizius, G. L.; Brédas, J.-L.; Collard, D. M. *J. Am. Chem. Soc.* **2012**, *134*, 7176. (f) Zafra, J. L.; Molina Ontoria, A.; Mayorga Burrezo, P.; Peña-Álvarez, M.; Samoc, M.; Szeremeta, J.; Ramírez, F. J.; Lovander, M. D.; Droske, C. J.; Pappenfus, T. M.; Echegoyen, L.; López Navarrete, J. T.; Martín, N.; Casado, J. *J. Am. Chem. Soc.* **2017**, *139*, 3095.
(6) (a) Bodwell, G. J.; Venkataramana, G.; Unikela, K. S. In *Fragments of Fullerenes and Carbon Nanotubes: Designed Synthesis, Unusual Reactions and Coordination Chemistry*; Petrukina, M., Scott, L. T., Eds.; Wiley-VCH: New York, 2011; chapter 14. (b) Ghasemabadi, P. G.; Yao, T.; Bodwell, G. J. *Chem. Soc. Rev.* **2015**, *44*, 6494.
(7) (a) Winnik, F. M. *Chem. Rev.* **1993**, *93*, 587. (b) Karuppannan, S.; Chambron, J.-C. *Chem. - Asian J.* **2011**, *6*, 964.
(8) (a) Figueira-Duarte, T. M.; Müllen, K. *Chem. Rev.* **2011**, *111*, 7260. (b) Casas-Solvas, J. M.; Howgego, J. D.; Davis, A. P. *Org. Biomol. Chem.* **2014**, *12*, 212.
(9) See, for instance: (a) Bodwell, G. J.; Bridson, J. N.; Houghton, T. J.; Kennedy, J. W. J.; Mannion, M. R. *Angew. Chem., Int. Ed. Engl.* **1996**, *35*, 1320. (b) Bodwell, G. J.; Bridson, J. N.; Houghton, T. J.; Kennedy, J. W. J.; Mannion, M. R. *Chem. - Eur. J.* **1999**, *5*, 1823. (c) Bodwell, G. J.; Bridson, J. N.; Cyrañski, M. K.; Kennedy, J. W. J.; Krygowski, T. M.; Mannion, M. R.; Miller, D. O. *J. Org. Chem.* **2003**, *68*, 2089. (d) Halling, M. D.; Unikela, K. S.; Bodwell, G. J.; Grant, D. M.; Pugmire, R. J. *J. Phys. Chem. A* **2012**, *116*, 5193. (e) Kahl, P.; Wagner, J.; Philipp; Balestrieri, C.; Becker, J.; Hausmann, H.; Bodwell, G. J.; Schreiner, P. R. *Angew. Chem., Int. Ed.* **2016**, *55*, 9277.
(10) Bodwell, G. J.; Fleming, J. J.; Mannion, M. R.; Miller, D. O. *J. Org. Chem.* **2000**, *65*, 5360.
(11) (a) Aprahamian, I.; Bodwell, G. J.; Fleming, J. J.; Manning, G. P.; Mannion, M. R.; Sheradsky, T.; Vermeij, R. J.; Rabinovitz, M. *J. Am. Chem. Soc.* **2003**, *125*, 1720. (b) Aprahamian, I.; Bodwell, G. J.; Fleming, J. J.; Manning, G. P.; Mannion, M. R.; Sheradsky, T.; Vermeij, R. J.; Rabinovitz, M. *Angew. Chem., Int. Ed.* **2003**, *42*, 2547. (c) Aprahamian, I.; Bodwell, G. J.; Fleming, J. J.; Manning, G. P.; Mannion, M. R.; Merner, B. L.; Sheradsky, T.; Vermeij, R. J.; Rabinovitz, M. *J. Am. Chem. Soc.* **2004**, *126*, 6765.
(12) For reviews, see: (a) van Zeist, W.-J.; Bickelhaupt, F. M. *Org. Biomol. Chem.* **2010**, *8*, 3118. (b) Fernández, I.; Bickelhaupt, F. M. *Chem. Soc. Rev.* **2014**, *43*, 4953. (c) Wolters, L. P.; Bickelhaupt, F. M. *WIREs Comput. Mol. Sci.* **2015**, *5*, 324.
(13) (a) von Hopffgarten, M.; Frenking, G. *WIREs Comput. Mol. Sci.* **2012**, *2*, 43. (b) Frenking, G.; Bickelhaupt, F. M. The EDA Perspective of Chemical Bonding. In *The Chemical Bond − Fundamental Aspects of Chemical Bonding*; Frenking, G., Shaik, S., Eds.; Wiley-VCH: Weinheim, 2014; pp 121−158.
(14) Representative examples on S_N2 and E2 reactions: (a) Bento, A. P.; Bickelhaupt, F. M. *J. Org. Chem.* **2007**, *72*, 2201. (b) Fernández, I.; Bickelhaupt, F. M.; Uggerud, E. *J. Org. Chem.* **2013**, *78*, 8574. (c) Wolters, L. P.; Ren, Y.; Bickelhaupt, F. M. *ChemistryOpen* **2014**, *3*, 29.
(15) Representative recent examples on pericyclic reactions: (a) Paton, R. S.; Kim, S.; Ross, A. G.; Danishefsky, S. J.; Houk, K. N. *Angew. Chem., Int. Ed.* **2011**, *50*, 10366. (b) Liu, F.; Paton, R. S.; Kim, S.; Liang, Y.; Houk, K. N. *J. Am. Chem. Soc.* **2013**, *135*, 15642. (c) Fernández, I. *Phys. Chem. Chem. Phys.* **2014**, *16*, 7662.
(16) (a) van Zeist, W.-J.; Bickelhaupt, F. M. *Dalton Trans.* **2011**, *40*, 3028 and references therein. (b) Wolters, L. P.; Bickelhaupt, F. M. *ChemistryOpen* **2013**, *2*, 106. (c) Green, A. G.; Liu, P.; Merlic, C. A.; Houk, K. N. *J. Am. Chem. Soc.* **2014**, *136*, 4575. (d) García-Rodeja, Y.; Fernández, I. *Chem. - Eur. J.* **2017**, *23*, 6634.
(17) (a) Fernández, I.; Solà, M.; Bickelhaupt, F. M. *Chem. - Eur. J.* **2013**, *19*, 7416. (b) Fernández, I.; Solà, M.; Bickelhaupt, F. M. *J. Chem. Theory Comput.* **2014**, *10*, 3863. (c) Bickelhaupt, F. M.; Solà, M.; Fernández, I. *Chem. - Eur. J.* **2015**, *21*, 5760. (d) García-Rodeja, Y.; Solà, M.; Fernández, I. *J. Org. Chem.* **2017**, *82*, 754. (e) García-Rodeja, Y.; Solá, M.; Bickelhaupt, F. M.; Fernández, I. *Chem. - Eur. J.* **2017**, DOI: 10.1002/chem.201701506.
(18) (a) García-Rodeja, Y.; Solà, M.; Bickelhaupt, F. M.; Fernández, I. *Chem. - Eur. J.* **2016**, *22*, 1368. (b) García-Rodeja, Y.; Solà, M.; Fernández, I. *Chem. - Eur. J.* **2016**, *22*, 10572.
(19) Frisch, M. J.; Trucks, G. W.; Schlegel, H. B.; Scuseria, G. E.; Robb, M. A.; Cheeseman, J. R.; Scalmani, G.; Barone, V.; Mennucci, B.; Petersson, G. A.; Nakatsuji, H.; Caricato, M.; Li, X.; Hratchian, H. P.; Izmaylov, A. F.; Bloino, J.; Zheng, G.; Sonnenberg, J. L.; Hada, M.; Ehara, M.; Toyota, K.; Fukuda, R.; Hasegawa, J.; Ishida, M.; Nakajima, T.; Honda, Y.; Kitao, O.; Nakai, H.; Vreven, T.; Montgomery, J. A., Jr.; Peralta, J. E.; Ogliaro, F.; Bearpark, M.; Heyd, J. J.; Brothers, E.; Kudin, K. N.; Staroverov, V. N.; Kobayashi, R.; Normand, J.; Raghavachari, K.; Rendell, A.; Burant, J. C.; Iyengar, S. S.; Tomasi, J.; Cossi, M.; Rega, N.; Millam, J. M.; Klene, M.; Knox, J. E.; Cross, J. B.; Bakken, V.; Adamo, C.; Jaramillo, J.; Gomperts, R.; Stratmann, R. E.; Yazyev, O.; Austin, A. J.; Cammi, R.; Pomelli, C.; Ochterski, J. W.; Martin, R. L.; Morokuma, K.; Zakrzewski, V. G.; Voth, G. A.; Salvador, P.; Dannenberg, J. J.; Dapprich, S.; Daniels, A. D.; Farkas, Ö.; Foresman, J. B.; Ortiz, J. V.; Cioslowski, J.; Fox, D. J. *Gaussian 09*, Revision D.01; Gaussian, Inc.: Wallingford, CT, 2009.
(20) (a) Becke, A. D. *J. Chem. Phys.* **1993**, *98*, 5648. (b) Lee, C.; Yang, W.; Parr, R. G. *Phys. Rev. B: Condens. Matter Mater. Phys.* **1988**, *37*, 785. (c) Vosko, S. H.; Wilk, L.; Nusair, M. *Can. J. Phys.* **1980**, *58*, 1200.
(21) Grimme, S.; Antony, J.; Ehrlich, S.; Krieg, H. *J. Chem. Phys.* **2010**, *132*, 154104.
(22) Weigend, F.; Ahlrichs, R. *Phys. Chem. Chem. Phys.* **2005**, *7*, 3297.
(23) McIver, J. W.; Komornicki, A. K. *J. Am. Chem. Soc.* **1972**, *94*, 2625.
(24) González, C.; Schlegel, H. B. *J. Phys. Chem.* **1990**, *94*, 5523.
(25) Zhao, Y.; Truhlar, D. G. *Theor. Chem. Acc.* **2008**, *120*, 215.
(26) (a) Miertuš, S.; Scrocco, E.; Tomasi, J. *Chem. Phys.* **1981**, *55*, 117. (b) Pascual-Ahuir, J. L.; Silla, E.; Tuñón, I. *J. Comput. Chem.* **1994**, *15*, 1127. (c) Barone, V.; Cossi, M. *J. Phys. Chem. A* **1998**, *102*, 1995.
(27) (a) Ess, D. H.; Houk, K. N. *J. Am. Chem. Soc.* **2007**, *129*, 10646. (b) Ess, D. H.; Houk, K. N. *J. Am. Chem. Soc.* **2008**, *130*, 10187. (c) Ess, D. H.; Jones, G. O.; Houk, K. N. *Org. Lett.* **2008**, *10*, 1633. For a recent review, see: (d) Bickelhaupt, F. M.; Houk, K. N. *Angew. Chem., Int. Ed.* **2017**, DOI: 10.1002/anie.201701486.
(28) Fernández, I.; Cossío, F. P.; Bickelhaupt, F. M. *J. Org. Chem.* **2011**, *76*, 2310.
(29) (a) Bodwell, G. J.; Miller, D. O.; Vermeij, R. J. *Org. Lett.* **2001**, *3*, 2093. See also: (b) Zhang, B.; Manning, G. P.; Dobrowolski, M. A.;

DOI: 10.1021/acs.joc.7b01449
J. Org. Chem. 2017, 82, 8157−8164

Cyranski, M. K.; Bodwell, G. J. *Org. Lett.* **2008**, *10*, 273. (c) Bodwell, G. J.; Vermeij, R. J. *Aust. J. Chem.* **2010**, *63*, 1703. (d) Zhang, B.; Zhao, Y.; Bodwell, G. J. *Synlett* **2016**, *27*, 2113. (e) Zhang, B.; Pascal, R. A., Jr.; Zhao, Y.; Bodwell, G. J. *Can. J. Chem.* **2017**, *95*, 460.

(30) The optimized structures of the transition states involved in the reactions of pyrenophanes **6** are given in Figure S1 in the Supporting Information.

(31) Johnson, E. R.; Keinan, S.; Mori-Sánchez, P.; Contreras-García, J.; Cohen, A. J.; Yang, W. *J. Am. Chem. Soc.* **2010**, *132*, 6498.

(32) Mitoraj, M. P.; Michalak, A.; Ziegler, T. *J. Chem. Theory Comput.* **2009**, *5*, 962.

(33) The EDA-NOCV calculations reported herein were carried out at the dispersion corrected BP86-D3/TZ2P level using the optimized B3LYP-D3/def2-SVP geometries with the ADF 2016 program package (www.scm.com). This level is therefore denoted BP86-D3/TZ2P//B3LYP-D3/def2-SVP.

DOI: 10.1021/acs.joc.7b01449
J. Org. Chem. 2017, 82, 8157−8164